Band-Edge Exciton Fine Structure of Small, Nearly Spherical Colloidal CdSe/ZnS Quantum Dots

Iwan Moreels,[†,‡,§,*] Gabriele Rainò,[†] Raquel Gomes,[‡,§] Zeger Hens,[‡,§] Thilo Stöferle,[†] and Rainer F. Mahrt[†,*]

[†]IBM Research—Zürich, Säumerstrasse 4, CH-8803 Rüschlikon, Switzerland, [‡]Physics and Chemistry of Nanostructures, Ghent University, Krijgslaan 281-S3, BE-9000 Ghent, Belgium, and [§]Center for Nano- and Biophotonics, Ghent University, Krijgslaan 281-S3, BE-9000 Ghent, Belgium

ABSTRACT The exciton fine structure of small (2—3.5 nm) wurtzite (WZ) and zincblende (ZB) CdSe quantum dots (Qdots) has been investigated by means of nanosecond and picosecond time-resolved photoluminescence spectroscopy, at temperatures ranging from 5 K to room temperature. For both crystal structures, we observe a similar dark—bright energy level splitting of 2.4—5 meV, with a larger splitting corresponding to smaller Qdots. In addition, spectrally resolved streak camera images collected at 5 K reveal the presence of a third state, split from the lower dark—bright manifold by 30—70 meV, again independently of the crystal structure of the Qdots. The data thus reveal that small WZ and ZB CdSe Qdots are optically indistinguishable. This contrasts with theoretical calculations within the effective-mass approximation, which, in the limit of spherical Qdots, yield a different fine structure for both. However, experimental and theoretical results converge when taking the Qdot shape into account. With transmission electron microscopy, we determined that our Qdots are prolate, with an aspect ratio of 1.15:1. Incorporating this value into our calculations, we obtain a similar fine structure for both WZ and ZB Qdots. Moreover, the opposite sign of the crystal field and shape anisotropy in CdSe suggests that the lowest energy level in small CdSe Qdots has an angular momentum projection $F = 0$, in contrast with (perfectly) spherical Qdots, where the lowest level corresponds to the dark ± 2 state. From the experimental and theoretical data we conclude that shape anisotropy and exchange interactions dominate over the crystal field anisotropy-induced splitting in this size range.

KEYWORDS: semiconductor nanocrystals · II—VI quantum dots · cadmium chalcogenide · optical properties

Colloidal semiconductor nanocrystals, or quantum dots (Qdots), are considered for a wide variety of photonic applications. They are used as biomarkers[1,2] and as active material in LEDs[3,4] and lasers.[5,6] They have also attracted interest as single photon sources for quantum information processing, due to the observation of room-temperature single-photon emission.[7,8] For the majority of these applications, a profound knowledge of the Qdot fine structure is crucial, as the energy and polarization of the emitted photons are determined by it. More recently, engineering of the energetic splitting between the band-edge energy levels down to values as low as 250 μeV has been demonstrated in quasi-type II CdSe/CdS Qdots.[9] This constitutes an important breakthrough in the fabrication of Qdot-based entangled photon sources and further highlights the pivotal role that the Qdot fine structure plays in novel photonic devices.

In colloidal Qdots the splitting between the band-edge energy levels has already been the subject of intense investigation. For instance, with time-resolved photoluminescence (PL) spectroscopy, a temperature-dependent exciton lifetime is observed, which has been modeled with a three-level system (a ground state and two excited states). This yielded a splitting of 1—5 meV between an energetically lower state with small oscillator strength and a higher state with larger oscillator strength.[10—14] Two routes are currently followed to interpret these results: in the fine structure model,[10—13,15] the emission is due to two distinct exciton states, with different total angular momentum projection F. The lower one has $F = \pm 2$; hence it is optically dark. The other corresponds to a bright state with $F = \pm 1^L$ (L denotes the lower of the two $F = \pm 1$ states[15]). The phonon model on the other hand proposes a phonon-assisted dark state transition that gives rise to a temperature-dependent PL.[14] The fine structure model has been further explored using time-resolved PL in magnetic field[16,17] (where a Zeeman splitting and mixing of the ± 2 dark and $\pm 1^L$ bright states are observed) and by cross-polarized third-order transient grating spectroscopy[18] (to monitor and model $+1$ to -1 spin flip processes in the Qdots).

At present, neither of the models satisfactorily describes all data. For instance, the observation of two zero-phonon emission lines (ZPL) in single Qdot PL experiments[12] favors the fine structure model, yet the theoretical magnitude of the splitting in spherical Qdots[15] is an order of magnitude larger than the experimentally observed one. On the other hand, the phonon model

* Address correspondence to iwan.moreels@ugent.be; rfm@zurich.ibm.com.

Received for review July 12, 2011 and accepted September 24, 2011.

Published online September 30, 2011
10.1021/nn202604z

is in quantitative agreement with the observed splitting in several Qdot materials,[14] yet it cannot account for the two ZPLs. The limited applicability of each individual model was highlighted by Liptay *et al.*,[19] who showed that both are needed for an accurate description of the line width of the first absorbance peak and the PL of CdSe Qdots, and the Stokes shift between both features.

The influence of Qdot shape anisotropy has largely been neglected in these studies. Indeed, already in the work of Efros *et al.*,[15] it has been concluded that CdSe Qdots can be regarded as spherical from an optical perspective, as the experimental aspect ratio led to a fine structure splitting that closely followed the calculations for spherical Qdots. Only for strongly anisotropic CdSe quantum rods (Qrods) has a different behavior been obtained experimentally.[20] The results agree with theoretical plane-wave pseudopotential calculations[21] and indicate that a smaller diameter d and larger aspect ratio AR lead to a reordering of the energy levels, with the lowest state having $F = 0$ instead of $F = \pm 2$. Yet, as the anisotropy-induced splitting scales with $(AR - 1)/d^2$,[15] the spherical approximation is assumed valid in most studies concerning (nearly) spherical Qdots, due to either a large d or an AR close to 1.

Here we address this issue by comparing the band-edge fine structure of small CdSe Qdots ($d = 2-3.5$ nm), emitting in the blue-green spectral region (480−550 nm) and synthesized with either a wurtzite (WZ) or zincblende (ZB) crystal structure. In the limit of spherical Qdots, both crystal structures have a different band-edge fine structure, which should allow to discriminate them. Furthermore, in this size range a pronounced shape effect should be present even for small deviations from sphericity.

Using time-resolved PL spectroscopy at cryogenic temperatures we demonstrate that WZ and ZB CdSe Qdots are optically indistinguishable. This unexpected result necessitates including shape anisotropy in the calculation of the exciton fine structure. Indeed, already for an AR of 1.15 (in nearly spherical Qdots, the experimental AR can be as high as 1.3[11,22,23]), the splitting induced by shape anisotropy dominates over the crystal field splitting present in WZ Qdots. Interestingly, from our calculations it turns out that the lowest state in small CdSe Qdots (<3 nm) is the dark 0^L state, similar to the results obtained on larger Qrods.[20,21]

RESULTS AND DISCUSSION

Transmission electron microscope (TEM) images of typical WZ and ZB CdSe core Qdots are shown in Figure 1a. They show that the Qdots are not perfectly spherical. Careful analysis of the Qdot shape for 3.1 nm WZ and 3.2 nm ZB Qdots yields an AR of 1.15 ± 0.1 for both crystal structures. The large standard deviation on the aspect ratio is not unexpected, as next to the shape distribution in the ensemble, a measurement of

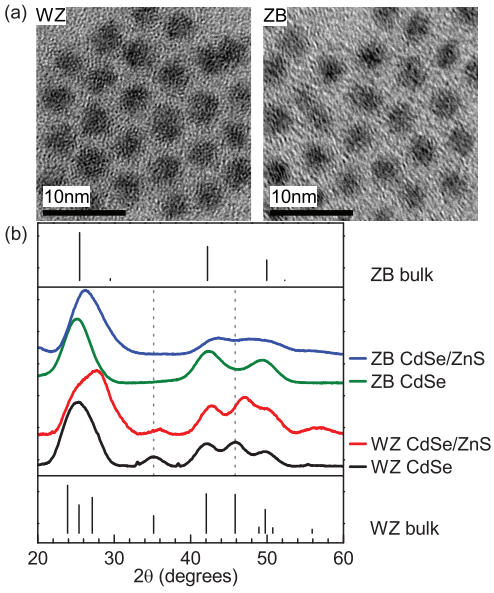

Figure 1. (a) TEM images of 3.1 nm WZ (left) and 3.2 nm ZB (right) CdSe Qdots. (b) XRD patterns of 2.9 nm WZ CdSe Qdots and 2.8 nm ZB Qdots (with and without ZnS shell). Dashed lines indicate the position of the $2\theta = 35.2°$ and 45.8° peak, present in WZ and absent in ZB Qdots. Theoretical bulk XRD patterns are given for WZ and ZB CdSe on the bottom and top of the graph, respectively.

the length of the major and minor axis is accurate only down to the distance between two atomic planes (we estimate a typical measurement error $\sigma_d \approx 0.25$ nm). TEM data on smaller Qdots were also collected (see Supporting Information). Here we obtain a similar AR of 1.16 ± 0.1 (2.3 nm WZ) and 1.18 ± 0.1 (2.0 nm ZB), respectively. Note however that here, the reported standard deviation might be a lower limit, as error propagation suggests that the intrinsic error on the measurement $\sigma_{AR} = \sqrt{2} \cdot AR(\sigma_d/d) \approx 0.2$. Nevertheless, for all samples, the reported average AR of 1.15−1.18 is significantly different from 1, as the error on the average AR $\sigma_{av} \approx 0.1 - 0.2/(50)^{1/2} = 0.014 - 0.028$.

To confirm that the Qdot crystal structure is WZ or ZB, respectively, we have measured X-ray diffraction (XRD) patterns (Figure 1b). The patterns from the Qdot cores clearly display the essential features that distinguish both: peaks can be observed at $2\theta = 35.2°$ and 45.8° in WZ Qdots; these peaks are absent in ZB Qdots. This confirms that the ZB Qdots are free of any WZ domains. Additionally, the equal amplitude of the 42.0° and 45.8° peaks in the WZ Qdots corresponds well with the theoretical ratio, confirming the purity of the WZ CdSe Qdots. Note that after shell growth, the pattern is slightly distorted due to the presence of ZnS, yet we observe no modification of ZB Qdots into WZ or *vice versa*. The preservation of the crystal structure is attributed to the low temperature of 140 °C used during the coating procedure.[24]

Detailed information on the energetic splitting of the band-edge exciton levels is obtained *via* time-resolved

PL spectroscopy. We performed two types of experiments. Spectrally integrated data were collected in the nanosecond time domain by time-correlated single photon counting with an avalanche photodiode, in a temperature range of 5 to 300 K, to confirm preexisting literature data on WZ CdSe Qdots and expand these to ZB Qdots. At 5 K, spectrally resolved measurements on a picosecond time scale by means of a streak camera allow to study more closely the fast decay processes occurring in the Qdots.

Spectrally integrated PL decay traces are shown in Figure 2. The data below 100 K are well fitted with a biexponential decay curve, yielding a short, response-time limited lifetime τ_S and a long lifetime τ_L. At 100 K, both components are merged into a single exponential decay with lifetime τ_L. Increasing the temperature further, an additional component with a lifetime of about 2−4 ns (depending on the sample; see Supporting Information) can be identified in the PL traces of the WZ Qdots (Figure 2a). It is also present in the ZB Qdots (Figure 2b), with a slightly higher amplitude and a similar lifetime of 2 ns. We attribute this component to thermally activated carrier trapping.[25] The stronger contribution in ZB Qdots is probably due to a lower room-temperature PL quantum yield of the ZB Qdots (16%) compared to WZ Qdots (21%). Note however that we typically observe an increase of the PL with decreasing temperature (see Supporting Information); hence carrier trapping is not expected to contribute strongly to the measurements at low temperature.

The fast component with lifetime τ_S arises from exciton relaxation within the fine structure following nonresonant excitation, which will be further discussed below. Focusing first on τ_L, we observe that it strongly decreases with temperature T. This can be explained by an energetically lower dark state a and a higher bright state b, with lifetimes τ_a and τ_b, respectively. Assuming a Boltzmann distribution between both states,[10] we can extract the energy difference δE_{ab} between the dark and bright state from τ_L (k_B is the Boltzmann constant):

$$\tau_L^{-1} = \frac{\tau_a^{-1} + \tau_b^{-1}}{2} + \frac{\tau_a^{-1} - \tau_b^{-1}}{2} \tanh \frac{\delta E_{ab}}{2k_B T} \quad (1)$$

Given the high repetition rate of the pump source, our time window is restricted to 12 ns. This implies that the largest τ_L values (at the lowest temperatures) may not be precisely defined, despite the fact that they are accurately obtained from a fit to the PL traces. However, taking into account that for colloidal Qdots the assumption $\tau_a^{-1} \ll \tau_b^{-1}$ holds, eq 1 can be reduced to

$$\tau_L^{-1} = \frac{\tau_b^{-1}}{2}\left(1 - \tanh \frac{\delta E_{ab}}{2k_B T}\right) \quad (2)$$

Restricting the analysis, due to the limited time window available, now to $\tau_L < 50$ ns, we can obtain

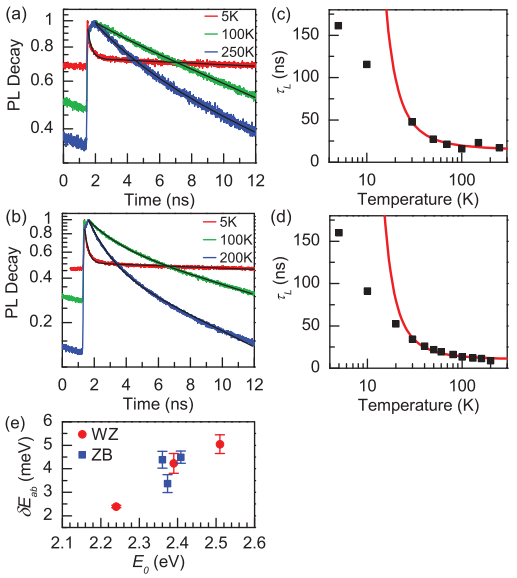

Figure 2. (a, b) Decay of the spectrally integrated PL for 2.5 nm WZ (a) and 2.6 nm ZB (b) Qdots. (c, d) The corresponding long lifetime τ_L of WZ (c) and ZB (d) Qdots decreases with temperature and shows similar values for both crystal structures. The fitted line in (c) and (d) stems from eq 2. (e) From the fit, the energetic splitting δE_{ab} between the lowest two states can be obtained.

δE_{ab} regardless of τ_a. For WZ CdSe Qdots we obtain 5.0 ± 0.4 meV (2.3 nm), 4.2 ± 0.4 meV (2.5 nm), and 2.4 ± 0.05 meV (3.3 nm), respectively, in agreement with literature data.[10−13] Values do not differ strongly from those obtained from a fit using eq 1, confirming that the exact value of τ_a does not strongly influence δE_{ab} here. For ZB Qdots, δE_{ab} equals 4.5 ± 0.3 meV (2.6 nm), 3.4 ± 0.4 meV (2.7 nm), and 4.4 ± 0.4 meV (2.8 nm), respectively. Figure 2e shows δE_{ab} as a function of the spectral position of the Qdot PL peak E_0 (determined at 5 K). The similar values obtained for both crystal structures reveal that WZ and ZB CdSe Qdots are optically indistinguishable on the nanosecond time scale. This is unexpected, as theoretical calculations using the effective mass approximation (EMA) yield a strongly different fine structure at the band-edge,[15] implying a different temperature dependence of the PL.

Further insight into this unexpected behavior is delivered by the spectrally resolved exciton recombination dynamics on a picosecond time scale. A typical streak camera image collected at 5 K shows two features (Figure 3a, 2.5 nm WZ Qdots). The band at lower energy arises from the slow decay of excitons in states a and b. Superimposed, at $t = 0$ ns we resolve a blue-shifted, rapidly decaying emission feature. We first demonstrate that this peak is an intrinsic feature of the Qdots, not related to Qdot−Qdot energy transfer, and is present even at low pump intensities; that is, it does not pertain to emission from biexcitons. To exclude energy transfer, we have prepared polystyrene films doped with 1 vol % of Qdots. This translates to an average Qdot center-to-center distance of 10 nm,

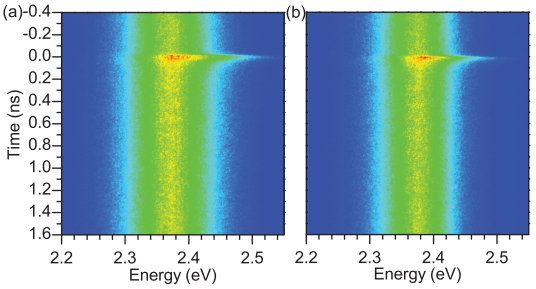

Figure 3. Streak camera images measured at 5 K for a close-packed (a) and a Qdot-doped polystyrene (b) film, respectively. Both images are highly similar, which allows to exclude energy transfer between Qdots contributing to the PL decay.

much larger than the interdot distance in close-packed films. Figure 3b shows that the streak camera image of the doped polystyrene film does not differ from a close-packed film, which demonstrates that the blue-shifted peak is intrinsic to the Qdots and is due to exciton recombination from a third state *c*. Streak camera images of 2.6 nm ZB Qdots as close-packed and 1 vol % doped polystyrene films confirm this result.

Power-dependent measurements on 3.0 nm ZB Qdots are shown in Figure 4. Spectral integration of the streak camera images (a typical image is shown in Figure 4a, using a pump intensity $I_0 = 0.1$ W/cm^2) yields the time-resolved PL decay, from which the amplitude A_c and lifetime τ_c of the *c*-state are extracted *via* a fit with the following equation: $I(t) = A_c \exp(-t/\tau_c) + y_0$ (Figure 4b). Figure 4c and d show that A_c scales linearly with the pump intensity, and τ_c is power-independent up to 2 W/cm^2. We conclude that under the low pump intensity of 50 mW/cm^2 used throughout this work, the *c*-state corresponds to a bright single-exciton state (a dark state would not be observable due to fast relaxation into the lower states), and biexcitons do not contribute to the PL. The creation of charged excitons (trions) is also safely excluded in our samples, as the PL corresponding to trion decay consists of a single peak, with a lifetime of about 1−5 ns.[13,26] Here we observe two emission features and a 54 ps lifetime for the fast component. A scheme of all states observed experimentally, with corresponding splitting energy, is shown in Figure 4e.

The streak camera images directly yield the energy splitting δE_{ac} between the blue-shifted PL peak and the lower energy PL band (Figure 5). At $t < 0$ ns, the luminescence comes predominantly from residual long-lived excitons in the lowest energy state *a*, excited by previous pulses in the pulse train. We take a 200 ps average (area 1 in Figure 5a) and fit the data with a bi-Gaussian peak function with maximum E_0, denoted $S(E_0)$. At $t = 0$ ns, an average is taken over a time window of 10 ps to fit the spectrum (arrows 2 in Figure 5a). Given the inhomogeneous line broadening of 100 meV (full width at half-maximum), determined from the

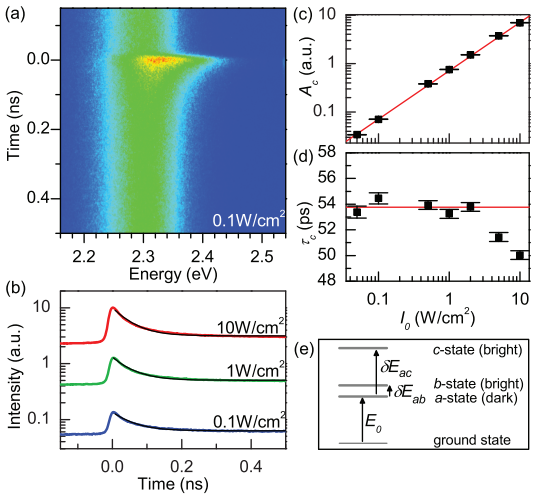

Figure 4. (a) Typical streak camera image, measured on 3.0 ZB Qdots at $I_0 = 0.1$ W/cm^2. (b) A fit (black line) to the spectrally integrated PL decay traces at different I_0 allows extraction of the amplitude A_c and lifetime τ_c of the fast component. (c) A_c increases linearly with I_0. (d) τ_c is I_0-independent up to 2 W/cm^2. Both results demonstrate that at $I_0 = 50$ mW/cm^2 we work in the single-exciton regime. (e) Energy level scheme including all states observed experimentally.

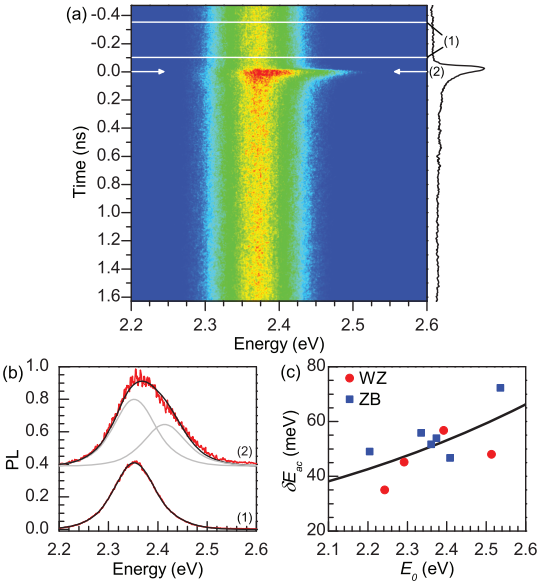

Figure 5. (a) Streak camera image at 5 K of 2.5 nm WZ CdSe Qdots. A projection of the PL decay is also shown. Markers (1) and (2) indicate the time windows taken to analyze the spectral position of the PL peaks. (b) The spectra before the pulse (1) arise from residual excitons excited by previous pulses. They are fitted to yield $S(E_0)$, which is then used to fit the data at $t = 0$ ns (2). (c) The resulting shift of the fast component δE_{ac} varies between 30 and 70 meV. The line serves as a guide to the eye.

width of the PL band at $t < 0$ ns, we can neglect the small splitting between the *a* and *b* state and consider them here as one effective state, with a PL peak shape and position given by $S(E_0)$. From the slow recombination time at 5 K of excitons in state *a*, we assume that

the amplitude for this peak is constant in this time window. A possible small contribution due to emission from state *b* is hereby neglected. The PL from the *c* state is characterized by $A \cdot S(E_0 + \delta E_{ac})$; that is, it consists of the same peak shape as the lower energy PL band, but may have a different (relative) amplitude *A* and is shifted to higher energy by a value δE_{ac}. As the inhomogeneous broadening is the same for all energy levels, using the same shape function *S* is justified. The resulting δE_{ac} for ZB and WZ Qdots is plotted as a function of E_0 in Figure 5b. Values increase from 30 to 70 meV as E_0 increases, consistent with the expected trend from EMA calculations,[15] but more importantly, we again observe no difference between both crystal structures.

Hence, by investigating the nano- and picosecond time scale exciton dynamics, we have resolved one dark state (*a*) and two bright states (*b* and *c*), with respective splitting energies δE_{ab} and δE_{ac}. To pinpoint the origin of the similar behavior for WZ and ZB Qdots, we have performed EMA calculations of the Qdot band-edge exciton fine structure. For WZ Qdots, we adopt the parameters from Efros *et al.*[15] The heavy hole and light hole effective mass along the *c*-axis ([002] direction) of the WZ crystal, $m_{hh} = 1.14m_e$ and $m_{lh} = 0.31m_e$, respectively, were determined by Norris *et al.* *via* a fit to the Qdot $1S_{3/2}1S_e$, $2S_{3/2}1S_e$, and $1P_{3/2}1P_e$ transitions.[27] They are in agreement with previous measurements on bulk CdSe.[28] For ZB Qdots, parameters are slightly different. We calculate a Bohr radius $a_B = 5.0$ nm, using the electron and hole effective masses of Kim *et al.*[29] and a CdSe dielectric constant $\varepsilon_0 = 10$. This value is slightly smaller than $a_B = 5.6$ nm in WZ CdSe. For the singlet−triplet splitting $\hbar\omega_{ST,ZB}$ in ZB CdSe, no literature data exist ($\hbar\omega_{ST,WZ} = 0.13$ meV in WZ CdSe[30]). However, we can estimate it from a_B using the empirical relation of Fu *et al.*[31] for bulk ZB semiconductors: $\hbar\omega_{ST,ZB} = 15.4/a_B^3$ ($\hbar\omega_{ST}$ in meV and a_B in nm). From this relation we obtain $\hbar\omega_{ST,ZB} = 0.12$ meV. The heavy hole and light hole effective mass, $m_{hh} = 0.9m_e$ and $m_{lh} = 0.18m_e$, respectively,[29] are taken along the [001] direction in analogy with the WZ Qdots and result in a light hole to heavy hole ratio $\beta = 0.2$.

Using these data we can calculate that, as expected, spherical CdSe WZ and ZB Qdots exhibit a strongly different band-edge fine structure (Figure 6a, WZ and Figure 6b, ZB). The exchange interaction Δ_{ex} splits the ZB Qdot energy levels into a 5-fold degenerate lower (dark) state and a 3-fold degenerate upper (bright) state, with the splitting energy scaling as $1/d^3$. In WZ Qdots, a constant crystal field anisotropy ($\Delta_{cr} = 25$ meV) further splits these states into five separate levels. The theory results in optically distinguishable crystal structures; for instance, the $\pm2-\pm1^L$ splitting clearly observed in WZ Qdots is absent in ZB Qdots. Further confirmation for the necessity to go beyond the spherical model follows from a comparison with the experimental data obtained from the spectrally integrated PL traces, as neither WZ nor ZB calculations show agreement with the $\delta E_{ab} = 2.4-5.0$ meV splitting obtained from the temperature-dependent PL decay traces.

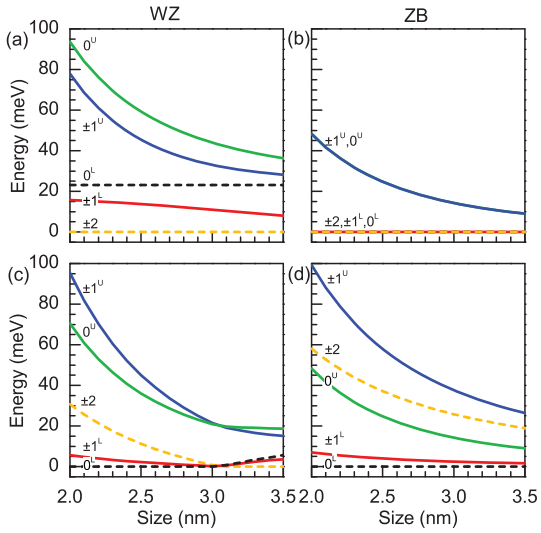

Figure 6. Theoretical calculation of the band-edge exciton fine structure for spherical WZ (a) and ZB (b) CdSe Qdots and prolate WZ (c) and ZB (d) Qdots with an AR of 1.15. In (c) and (d) the fine structure is more similar for both, due to the reduced influence of crystal field splitting compared to anisotropy-induced splitting. Dark states are marked by dotted lines; bright states by full lines.

By additionally including the interaction due to an anisotropic shape Δ_{sh} and using the experimentally observed AR of 1.15, the difference between WZ and ZB Qdots is strongly reduced (Figure 6c, WZ and Figure 6d, ZB). First, below a size of 3 nm, a crossover of the lowest states occurs in WZ Qdots, resulting in the dark 0^L state becoming the lowest energy level. This is peculiar to the case of prolate WZ Qdots, due to the opposite sign of Δ_{cr} and Δ_{sh}. Consequently, as Δ_{sh} is also negative in ZB Qdots, the fine structure levels for both WZ and ZB Qdots show the same order and scaling with Qdot size. Second, in WZ Qdots the $0^L-\pm1^L$ splitting is strongly reduced when increasing the anisotropy, again due to the opposite sign of Δ_{cr} and Δ_{sh}. As a result, we obtain a splitting δE_{ab} of 3.6 meV (2.3 nm WZ Qdots) to 2.4 meV (3.3 nm), far smaller than the 14.7−9.2 meV range obtained for spherical WZ Qdots. On the other hand, for ZB Qdots with an AR of 1.15, the lowest levels are no longer degenerate. The resulting $0^L-\pm1^L$ splitting varies from 4.9 meV (2.3 nm WZ Qdots) to 1.9 meV (3.3 nm). Hence, values are highly similar to WZ Qdots, and for both crystal structures, calculations now indeed show better agreement with experimental data ($\delta E_{ab} = 2.4-5.0$ meV). The 0^L-0^U splitting in ZB Qdots is slightly smaller than in WZ Qdots, mainly due to the smaller a_B; yet the difference with WZ Qdots is within the resolution of the experimental data (Figure 5c).

The calculated band-edge energy level splitting is thus in good agreement with experimental results.

The similarity of the calculated data shows that for the WZ Qdots Δ_{cr} plays only a minor role in this size range. Due to the strong increase of Δ_{sh} in small CdSe Qdots (it scales with $1/d^2$), Δ_{cr} is perfectly canceled by Δ_{sh} for 3 nm WZ Qdots and becomes even 2.5 times weaker in 2 nm Qdots. Note that we do not aim for a quantitative comparison with experimental data. The EMA calculations might overestimate the splitting, due to the infinite potential barriers at the Qdot surface. Furthermore, due to the large fraction of surface atoms in this size range, the EMA might be no longer strictly valid,[15] and more advanced calculations, for instance using the semiempirical plane-wave pseudopotential method reported by Zhao *et al.*,[21] are required. Their results on anisotropic WZ Qrods indeed support our conclusions, although they observe the $\pm 2-0^L$ crossover behavior only for an AR larger than 1.3.

Interestingly, the necessity to include shape anisotropy, evidenced by direct measurement of the AR using TEM and by the results obtained with PL spectroscopy, differentiates our WZ Qdots from those used by Efros *et al.*,[15] even though both are composed of the same CdSe material. TEM and optical data revealed that their synthesized small WZ CdSe Qdots have an AR close to 1, which resulted in optical properties that agree well with EMA calculations for spherical Qdots. It highlights that different synthesis protocols easily yield differently shaped Qdots; consequently, care must be taken when extrapolating the corresponding opto-electronic properties.

In conclusion, the influence of shape has only been discussed before in the case of highly anisotropic Qrods.[21] Here, we demonstrate that a small Qdot size yields a similar effect; it strongly enhances Δ_{ex} and Δ_{sh}, rendering them the major contribution to the fine structure splitting in nearly spherical Qdots. The theoretical calculations also allow us to assign the *a*, *b*, and *c* states. In agreement with results on the Qrods, our data suggest that the lowest state corresponds to the dark 0^L state. States *b* and *c* correspond to the bright $\pm 1^L$ and 0^U state, respectively. Other states are not observed experimentally, possibly due to strong competition with nonradiative relaxation into the lower states.

The results presented here have important consequences for the fundamental understanding of the opto-electronic properties of colloidal Qdots, obtained by for instance magnetic field dependent PL[16,17] or third-order transient grating spectroscopy.[18] At present, most experiments are conducted on large CdSe Qdots. However, current models need to be reconsidered when similar data are measured on Qdots within the 2−3.5 nm size range.

METHODS

Synthesis and Structural Characterization. To prepare CdSe/ZnS core−shell Qdots, WZ and ZB CdSe cores were synthesized according to literature procedures.[24,32] Hereafter, Qdots were coated with a ZnS shell at 140 °C[24] in order to prevent a modification of the crystal structure during shell growth. We measured X-ray diffraction patterns to confirm the crystal structure of the samples. TEM images were collected on Qdots of different size, and we analyzed the Qdot shape for 3.1 nm WZ and 3.2 nm ZB Qdots. For each sample, 50 Qdots were fitted with an ellipse, which yielded the length of the major and minor axis and thus the Qdot AR. A similar analysis is performed on 2.3 nm WZ and 2.0 nm ZB Qdots (see Supporting Information).

PL Measurements. Two types of films are prepared, both on a glass substrate: either the Qdots are dropcasted from a toluene solution (close-packed film), or they are first mixed with a solution of polystyrene (5 m%) in toluene and subsequently spin-coated (1vol % Qdot-doped polymer film). For the optical characterization, the samples are mounted in a helium cryostat and investigated in a temperature range between 5 and 300 K. They are excited at 400 nm by a frequency-doubled 80 MHz Ti:Sa femtosecond pulsed laser. Time-resolved PL data are collected by time-correlated single-photon counting, to investigate the spectrally integrated nanosecond dynamics, or a streak camera, which yields the spectrally resolved picosecond dynamics. All measurements are performed with a low pump intensity I_0 of 50 mW/cm^2 to ensure that we work in the single-exciton regime. Power-dependent measurements up to 10 W/cm^2 indeed yield a linear increase of the PL with I_0, with an I_0-independent decay constant up to 2 W/cm^2.

Acknowledgment. I.M. is a researcher with the FWO-Vlaanderen. This project is funded by the EU Seventh Framework Program (EU-FP7 ITN Herodot). Z.H. acknowledges funding from the Belgian Science Policy Office (IAP 6.10 photonics@be). O. Janssens (Department of Solid State Sciences, Ghent University) is acknowledged for technical support (XRD measurements).

Supporting Information Available: TEM analysis of the Qdot shape and data on the temperature-dependent photoluminescence lifetime, quantum yield, and carrier trapping. This material is available free of charge *via* the Internet at http://pubs.acs.org.

REFERENCES AND NOTES

1. Michalet, X.; Pinaud, F. F.; Bentolila, L. A.; Tsay, J. M.; Doose, S.; Li, J. J.; Sundaresan, G.; Wu, A. M.; Gambhir, S. S.; Weiss, S. Quantum Dots for Live Cells, in Vivo Imaging, and Diagnostics. *Science* **2005**, *307*, 538–544.
2. Gill, R.; Zayats, M.; Willner, I. Semiconductor Quantum Dots for Bioanalysis. *Angew. Chem., Int. Ed.* **2008**, *47*, 7602–7625.
3. Rogach, A. L.; Gaponik, N.; Lupton, J. M.; Bertoni, C.; Gallardo, D. E.; Dunn, S.; Pira, N. L.; Paderi, M.; Repetto, P.; Romanov, S. G.; *et al.* Light-Emitting Diodes with Semiconductor Nanocrystals. *Angew. Chem., Int. Ed.* **2008**, *47*, 6538–6549.
4. Anikeeva, P. O.; Halpert, J. E.; Bawendi, M. G.; Bulović, V. Quantum Dot Light-Emitting Devices with Electroluminescence Tunable over the Entire Visible Spectrum. *Nano Lett.* **2009**, *9*, 2532–2536.
5. Eisler, H. J.; Sundar, V. C.; Bawendi, M. G.; Walsh, M.; Smith, H. I.; Klimov, V. Color-Selective Semiconductor Nanocrystal Laser. *Appl. Phys. Lett.* **2002**, *80*, 4614–4616.
6. Zavelani-Rossi, M.; Lupo, M. G.; Krahne, R.; Manna, L.; Lanzani, G. Lasing in Self-Assembled Microcavities of CdSe/CdS Core/Shell Colloidal Quantum Rods. *Nanoscale* **2010**, *2*, 931–935.

7. Brokmann, X.; Giacobino, E.; Dahan, M.; Hermier, J. P. Highly Efficient Triggered Emission of Single Photons by Colloidal CdSe/ZnS Nanocrystals. *Appl. Phys. Lett.* **2004**, *85*, 712–714.
8. Mahler, B.; Spinicelli, P.; Buil, S.; Quelin, X.; Hermier, J.; Dubertret, B. Towards Non-Blinking Colloidal Quantum Dots. *Nat. Mater.* **2008**, *7*, 659–664.
9. Brovelli, S.; Schaller, R.; Crooker, S.; García-Santamaría, F.; Chen, Y.; Viswanatha, R.; Hollingsworth, J.; Htoon, H.; Klimov, V. Nano-Engineered Electron.Hole Exchange Interaction Controls Exciton Dynamics in Core.Shell Semiconductor Nanocrystals. *Nat. Commun.* **2011**, *2*, 280.
10. Labeau, O.; Tamarat, P.; Lounis, B. Temperature Dependence of the Luminescence Lifetime of Single CdSe/ZnS Quantum Dots. *Phys. Rev. Lett.* **2003**, *90*, 257404.
11. de Mello Donegá, C.; Bode, M.; Meijerink, A. Size- and Temperature-Dependence of Exciton Lifetimes in CdSe Quantum Dots. *Phys. Rev. B* **2006**, *74*, 085320.
12. Biadala, L.; Louyer, Y.; Tamarat, P.; Lounis, B. Direct Observation of the Two Lowest Exciton Zero-Phonon Lines in Single CdSe/ZnS Nanocrystals. *Phys. Rev. Lett.* **2009**, *103*, 037404.
13. Fernée, M. J.; Littleton, B. N.; Rubinsztein-Dunlop, H. Detection of Bright Trion States Using the Fine Structure Emission of Single CdSe/ZnS Colloidal Quantum Dots. *ACS Nano* **2009**, *3*, 3762–3768.
14. Oron, D.; Aharoni, A.; de Mello Donegá, C.; van Rijssel, J.; Meijerink, A.; Banin, U. Universal Role of Discrete Acoustic Phonons in the Low-Temperature Optical Emission of Colloidal Quantum Dots. *Phys. Rev. Lett.* **2009**, *102*, 177402.
15. Efros, A. L.; Rosen, M.; Kuno, M.; Nirmal, M.; Norris, D. J.; Bawendi, M. Band-Edge Exciton in Quantum Dots of Semiconductors with a Degenerate Valence Band: Dark and Bright Exciton States. *Phys. Rev. B* **1996**, *54*, 4843–4856.
16. Johnston-Halperin, E.; Awschalom, D. D.; Crooker, S. A.; Efros, A. L.; Rosen, M.; Peng, X.; Alivisatos, A. P. Spin Spectroscopy of Dark Excitons in CdSe Quantum Dots to 60 T. *Phys. Rev. B* **2001**, *63*, 205309.
17. Furis, M.; Hollingsworth, J. A.; Klimov, V. I.; Crooker, S. A. Time- and Polarization-Resolved Optical Spectroscopy of Colloidal CdSe Nanocrystal Quantum Dots in High Magnetic Fields. *J. Phys. Chem. B* **2005**, *109*, 15332–15338.
18. Wong, C. Y.; Kim, J.; Nair, P. S.; Nagy, M. C.; Scholes, G. D. Relaxation in the Exciton Fine Structure of Semiconductor Nanocrystals. *J. Phys. Chem. C* **2009**, *113*, 795–811.
19. Liptay, T. J.; Marshall, L. F.; Rao, P. S.; Ram, R. J.; Bawendi, M. G. Anomalous Stokes Shift in CdSe Nanocrystals. *Phys. Rev. B* **2007**, *76*, 155314.
20. Le Thomas, N.; Herz, E.; Schöps, O.; Woggon, U.; Artemyev, M. V. Exciton Fine Structure in Single CdSe Nanorods. *Phys. Rev. Lett.* **2005**, *94*, 016803.
21. Zhao, Q.; Graf, P. A.; Jones, W. B.; Franceschetti, A.; Li, J.; Wang; Kim, K. Shape Dependence of Band-Edge Exciton Fine Structure in CdSe Nanocrystals. *Nano Lett.* **2007**, *7*, 3274–3280.
22. Murray, C. B.; Norris, D. J.; Bawendi, M. G. Synthesis and Characterization of Nearly Monodisperse CdE (E = Sulfur, Selenium, Tellurium) Semiconductor Nanocrystallites. *J. Am. Chem. Soc.* **1993**, *115*, 8706–8715.
23. Shiang, J. J.; Kadavanich, A. V.; Grubbs, R. K.; Alivisatos, A. P. Symmetry of Annealed Wurtzite CdSe Nanocrystals: Assignment to the C3v Point Group. *J. Phys. Chem.* **1995**, *99*, 17417–17422.
24. Capek, R. K.; Lambert, K.; Dorfs, D.; Smet, P. F.; Poelman, D.; Eychmuller, A.; Hens, Z. Synthesis of Extremely Small CdSe and Bright Blue Luminescent CdSe/ZnS Nanoparticles by a Prefocused Hot-Injection Approach. *Chem. Mater.* **2009**, *21*, 1743–1749.
25. Jones, M.; Lo, S. S.; Scholes, G. D. Signatures of Exciton Dynamics and Carrier Trapping in the Time-Resolved Photoluminescence of Colloidal CdSe Nanocrystals. *J. Phys. Chem. C* **2009**, *113*, 18632–18642.
26. Louyer, Y.; Biadala, L.; Tamarat, P.; Lounis, B. Spectroscopy of Neutral and Charged Exciton States in Single CdSe/ZnS Nanocrystals. *Appl. Phys. Lett.* **2010**, *96*, 203111.
27. Norris, D. J.; Bawendi, M. G. Measurement and Assignment of the Size-Dependent Optical Spectrum in CdSe Quantum Dots. *Phys. Rev. B* **1996**, *53*, 16338–16346.
28. Hopfield, J. J. Exciton States and Band Structure in CdS and CdSe. *J. Appl. Phys.* **1961**, *32*, 2277–2281.
29. Kim, Y. D.; Klein, M. V.; Ren, S. F.; Chang, Y. C.; Luo, H.; Samarth, N.; Furdyna, J. K. Optical Properties of Zinc-Blende CdSe and ZnxCd1-xSe Films Grown on GaAs. *Phys. Rev. B* **1994**, *49*, 7262–7270.
30. Kiselev, V. A.; Razbirin, B. S.; Uraltsev, I. N. Additional Waves and Fabry-Perot Interference of Photoexcitons (Polaritons) in Thin II-VI Crystals. *Phys. Status Solidi B* **1975**, *72*, 161–172.
31. Fu, H.; Wang, L.; Zunger, A. Excitonic Exchange Splitting in Bulk Semiconductors. *Phys. Rev. B* **1999**, *59*, 5568–5574.
32. Carbone, L.; Nobile, C.; Giorgi, M. D.; Sala, F. D.; Morello, G.; Pompa, P.; Hytch, M.; Snoeck, E.; Fiore, A.; Franchini, I. R.; Nadasan, M.; Silvestre, A. F.; Chiodo, L.; Kudera, S.; Cingolani, R.; *et al.* Synthesis and Micrometer-Scale Assembly of Colloidal CdSe/CdS Nanorods Prepared by a Seeded Growth Approach. *Nano Lett.* **2007**, *7*, 2942–2950.